UnfoldLDM: Deep Unfolding-based Blind Image Restoration with Latent Diffusion Priors

Chunming He^{1,*}, Rihan Zhang^{1,*}, Zheng Chen², Bowen Yang³, Chengyu Fang⁴, Yunlong Lin⁵, Fengyang Xiao^{1,†}, and Sina Farsiu^{1,†} Duke University, ²Shanghai Jiao Tong University, ³Peking University, ⁴Tsinghua University, ⁵Xiamen University,

* Equal Contribution, † Corresponding Author, Contact: chunming.he@duke.edu.

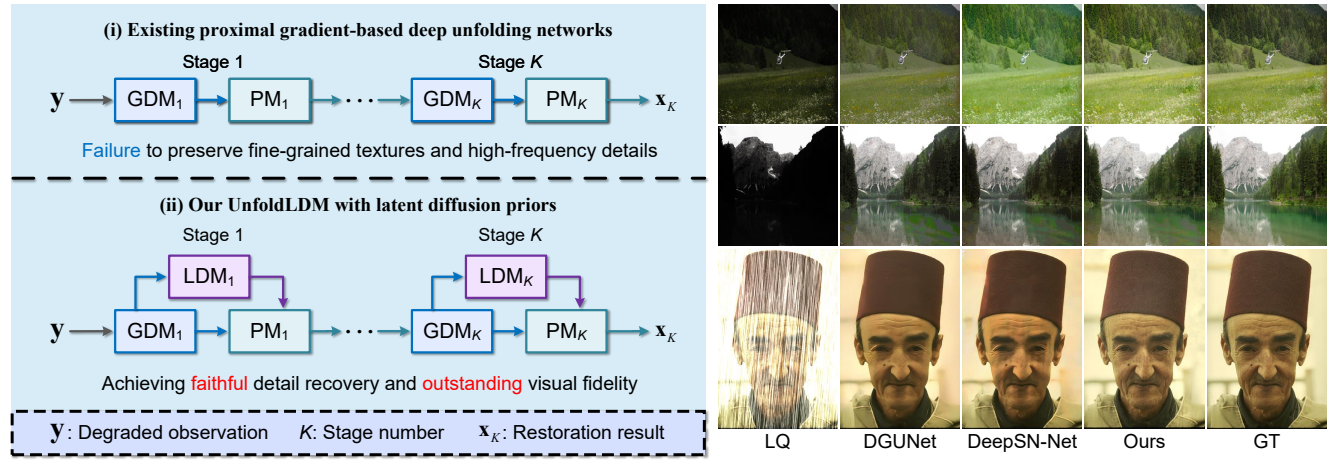


Figure 1. Comparison between existing proximal gradient-based DUN-based methods (*e.g.*, DGUNet [44] and DeepSN-Net [7]) and our UnfoldLDM. UnfoldLDM better resists unknown degradation and eliminates the over-smoothing bias that existing DUNs suffer.

Abstract

Deep unfolding networks (DUNs) combine the interpretability of model-based methods with the learning ability of deep networks, yet remain limited for blind image restoration (BIR). Existing DUNs suffer from: (1) Degradation-specific dependency, as their optimization frameworks are tied to a known degradation model, making them unsuitable for BIR tasks; and (2) Over-smoothing bias, resulting from the direct feeding of gradient descent outputs, dominated by low-frequency content, into the proximal term, suppressing fine textures. To overcome these issues, we propose UnfoldLDM to integrate DUNs with latent diffusion model (LDM) for BIR. In each stage, UnfoldLDM employs a multi-granularity degradation-aware (MGDA) module as the gradient descent step. MGDA models BIR as an unknown degradation estimation problem and estimates both the holistic degradation matrix and its decomposed forms, enabling robust degradation removal. For the proximal step, we design a degradation-resistant LDM (DR-LDM) to extract compact degradation-invariant priors from the MGDA output. Guided by this prior, an oversmoothing correction transformer (OCFormer) explicitly recovers high-frequency components and enhances texture details. This unique combination ensures the final result is degradation-free and visually rich. Experiments show that our UnfoldLDM achieves a leading place on various BIR tasks and benefits downstream tasks. Moreover, our design is compatible with existing DUN-based methods, serving as a plug-and-play framework. Code will be released.

1. Introduction

Blind image restoration (BIR) aims to recover high-quality images from unknown degradations [20, 31, 32, 56, 70–73]. It plays a vital role in numerous applications, including photography [19, 39, 74], medical imaging [37, 38, 47], and downstream vision tasks [6, 22, 78]. Traditional methods based on handcrafted priors are interpretable but struggle to generalize to real-world degradations [27], whereas learning-based methods achieve superior performance but often lack interpretability [4, 19].

Deep unfolding networks (DUNs) have emerged as a promising paradigm to bridge this gap [53]. By unfolding

the iterative optimization into a multi-stage network, DUNs inherit the model-based interpretability while leveraging the learning-based representational power. Among them, proximal-gradient (PG)-based DUNs are widely adopted for their flexibility and effectiveness [23, 24]. As shown in Fig. 1, a typical PG-based DUN alternates between a gradient descent step derived from the observation model and a proximal operator parameterized by a learnable prior, enforcing data fidelity while enhancing perceptual quality.

However, existing PG-based DUNs face two major challenges: (1) Degradation-specific dependency. Most are designed for a particular degradation type (e.g., deblurring or low-light enhancement) and rely on known physical priors, making them unsuitable for complex or mixed degradations. (2) Over-smoothing bias. Due to the dominance of low-frequency information in degraded images, gradient updates primarily recover coarse structures while neglecting high-frequency details. As the learnable step size converges to small updates, high-frequency textures are further suppressed or mistaken for noise, bringing over-smoothed outputs with reduced structural fidelity (see Fig. 1).

To overcome these, we propose UnfoldLDM, which first integrates DUNs with the latent diffusion model (LDM) for BIR. Each stage in UnfoldLDM has two components: (i) a multi-granularity degradation-aware (MGDA) module serving as the gradient descent term, and (ii) a proximal design comprising a Degradation-Resistant LDM (DR-LDM) and an over-smoothing correction transformer (OCFormer).

In MGDA, we formulate BIR as an unknown degradation estimation problem by jointly estimating the holistic degradation matrix and its decomposed factors. The consistency between these two representations is guaranteed by an intra-stage degradation-aware (ISDA) loss. Solving these two forms in tandem ensures both scalability and stability, thereby facilitating robust degradation removal.

For the proximal step, DR-LDM extracts compact degradation-invariant priors from the MGDA output, leveraging generative capacity to preserve high-frequency information. Guided by this prior, OCFormer explicitly restores fine-grained texture details suppressed in the earlier period. As unfolding progresses, MGDA increasingly captures degradation patterns, while DR-LDM and OCFormer progressively refine texture recovery, ensuring results that are both degradation-free and visually rich.

Our contributions are summarized as follows:

- (1) We propose UnfoldLDM, the first method that integrates DUNs with latent diffusion priors for BIR, mitigating degradation-specific dependence and over-smoothing bias.
- (2) We propose the MGDA module, which jointly estimates holistic and decomposed degradation forms. An ISDA loss is further introduced to ensure consistent degradation estimation, enabling robust and stable restoration.
- (3) We design a DR-LDM to extract a compact degradation-

invariant prior, which guides OCFormer to explicitly recover high-frequency textures.

(4) Experiments across diverse BIR tasks and downstream applications validate our superiority, generalizability, and plug-and-play compatibility with existing methods.

2. Related Works

DUN-based image restoration. DUNs [21, 23] translate iterative optimization into trainable architectures, enabling effective modeling of low-level vision tasks such as deblurring [44], super-resolution [68], and low-light enhancement[23]. Most DUNs adopt a proximal gradient scheme, combining a gradient descent step with a proximal operator. However, when applied to BIR, they face two major challenges: (i) the degradation-specific design limits generalization to unknown degradations, and (ii) the strong coupling between descent and proximal terms biases recovery toward low-frequency components, leading to oversmoothed results. This highlights the need for degradationagnostic DUNs that preserve fine structural details.

Prior-guided image restoration. Image priors are crucial for constraining solution spaces in restoration. Classical handcrafted priors, such as total variation [2, 14], lack robustness under real-world degradations, while deep generative priors from GANs [15, 16, 20], VAEs [6, 13], and diffusion models [56, 63, 64] capture richer natural statistics and yield realistic results. However, these priors can be misled by heavily degraded inputs, leading to false restoration. A promising direction is to couple degradation-aware modeling with generative priors, enabling texture-preserving restoration with data fidelity. Following this, our UnfoldLDM integrates latent diffusion priors into a degradation-aware DUN, effectively addressing the above issues.

3. Restoration Model and Optimization

Restoration model. Blind image restoration (BIR) is an ill-posed inverse problem. Given the degraded observation $\mathbf{y} \in \mathbb{R}^{c \times h \times w}$, the degradation process can be formulated

$$\mathbf{y} = \mathbf{D}\mathbf{x} + \mathbf{n},\tag{1}$$

 $\mathbf{y} = \mathbf{D}\mathbf{x} + \mathbf{n}, \tag{1}$ where $\mathbf{x} \in \mathbb{R}^{c \times h \times w}$ is the latent clean image, $\mathbf{D} \in$ $\mathbb{R}^{c \times hw \times hw}$ is the unknown degradation matrix, and \mathbf{n} is additive noise. The objective is to recover the optimal clean image by minimizing the following energy:

$$L(\mathbf{x}) = \frac{1}{2} \|\mathbf{y} - \mathbf{D}\mathbf{x}\|_{2}^{2} + \lambda \phi(\mathbf{x}), \tag{2}$$

where $\|\cdot\|_2^2$ is the l_2 -norm, $\phi(\cdot)$ denotes a regularization term learned by deep networks to encode prior knowledge, and λ is a hyper-parameter balancing these two terms..

To address the complexity of blind settings and improve modeling efficiency, we introduce a structured decomposition of the holistic degradation matrix **D** into two spatially

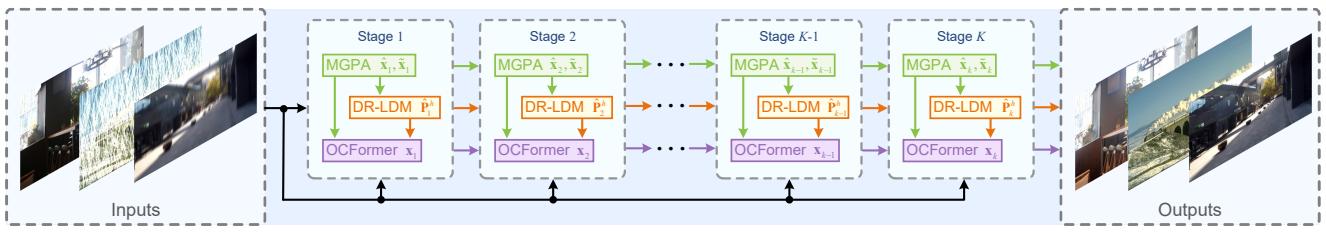


Figure 2. Framework of our proposed UnfoldLDM.

decoupled matrices, $\mathbf{W} \in \mathbb{R}^{c \times h \times h}$ and $\mathbf{M} \in \mathbb{R}^{c \times w \times w}$:

$$\mathbf{D} = \mathbf{M}^T \otimes \mathbf{W},\tag{3}$$

where \otimes denotes the Kronecker product.

This factorization is more efficient than directly learning \mathbf{D} , whose dimension grows quadratically with image resolution. Also, the decomposed ones enhance structure awareness: \mathbf{W} captures spatial transformations, while \mathbf{M} models spectral or directional distortions. Integrating both the holistic form \mathbf{D} and the decomposed form (\mathbf{W}, \mathbf{M}) enables expressive modeling of complex degradations while maintaining efficiency. The final objective function is:

$$L(\mathbf{x}) = \frac{1}{2} \|\mathbf{y} - \mathbf{D}\mathbf{x}\|_{2}^{2} + \frac{1}{2} \|\mathbf{y} - \mathbf{W}\mathbf{x}\mathbf{M}\|_{2}^{2} + \lambda \phi(\mathbf{x}).$$
(4)

Model optimization. To minimize Eq. (4), we employ proximal gradient algorithm [44]. At the k^{th} iteration $(1 \le k \le K)$, the optimization problem can be expressed

$$\mathbf{x}_{k} = \arg\min_{\mathbf{x}} \ \frac{1}{2} \|\mathbf{y} - \mathbf{D}\mathbf{x}\|_{2}^{2} + \frac{1}{2} \|\mathbf{y} - \mathbf{W}\mathbf{x}\mathbf{M}\|_{2}^{2} + \lambda \phi(\mathbf{x}). \tag{5}$$

Unlike conventional formulations that involve a single gradient and a proximal step, our setting requires customized treatment for both holistic and decomposed degradations to enhance flexibility. Accordingly, each iteration consists of two gradient descent steps (corresponding to the two fidelity terms) and one proximal step. We define:

$$g(\mathbf{x}) = \frac{1}{2} \|\mathbf{y} - \mathbf{D}\mathbf{x}\|_{2}^{2}, \ h(\mathbf{x}) = \frac{1}{2} \|\mathbf{y} - \mathbf{W}\mathbf{x}\mathbf{M}\|_{2}^{2}.$$
 (6)

Let the intermediate solutions for the two gradient updates be $\hat{\mathbf{x}}_k$ and $\tilde{\mathbf{x}}_k$, yielding:

$$\hat{\mathbf{x}}_{k} = \mathbf{x}_{k-1} - \beta \nabla g(\mathbf{x}_{k-1}),$$

$$= \mathbf{x}_{k-1} - \beta \mathbf{D}^{T} (\mathbf{D} \mathbf{x}_{k-1} - \mathbf{y}),$$
(7)

$$\tilde{\mathbf{x}}_{k} = \mathbf{x}_{k-1} - \gamma \nabla h(\mathbf{x}_{k-1}),$$

$$= \mathbf{x}_{k-1} - \gamma \mathbf{W}^{T} (\mathbf{W} \mathbf{x}_{k-1} \mathbf{M} - \mathbf{y}) \mathbf{M}^{T},$$
(8)

$$\mathbf{x}_k = \operatorname{prox}_{\lambda, \phi}(\hat{\mathbf{x}}_k, \tilde{\mathbf{x}}_k), \tag{9}$$

where β and γ are two step-size parameters. This enables both global degradation modeling through **D** and structure-aware refinement via (\mathbf{W}, \mathbf{M}) , resulting in complementary gradient updates that jointly improve restoration quality.

4. UnfoldLDM

We unfold the iterative optimization process into a multistage network, UnfoldLDM. As shown in Figs. 2 and 3, each stage, corresponding to one iteration of the model-based solver, has three main components, including a multigranularity degradation-aware (MGDA) module as the gradient descent term and a proximal operator composed of a degradation-resistant latent diffusion model (DR-LDM) and an over-smoothing correction transformer (OCFormer). As the unfolding proceeds, these modules collaboratively refine degradation estimation and enhance texture recovery, producing visually rich and degradation-free results.

In practice, UnfoldLDM is trained in two phases to encourage the DR-LDM to generate high-quality priors.

4.1. Phase I: Pretrain UnfoldLDM

We first pretrain UnfoldLDM to encode clean images into compact priors through a Prior Inference (PI) module, and use these priors to guide OCFormer for detail reconstruction. This allows the network to learn what type of prior information benefits fine-detail recovery. The extracted "GT" priors then supervise DR-LDM in producing similar high-quality priors at Phase II when the input is degraded.

MGDA. MGDA follows the gradient terms in Eqs. (7) and (8), with the fixed β and γ learnable. Given that degradation is unknown, MGDA adopts a data-driven formulation to estimate degradation operators and the corresponding gradients. At stage k, two Siamesed Visual State Space (VSS) blocks [18], termed $VSS_k^{\mathbf{D}}(\bullet)$ and $VSS_k^{\mathbf{D}^T}(\bullet)$, are used to simulate \mathbf{D} and \mathbf{D}^T . Thus, Eq. (7) can be rewritten

$$\hat{\mathbf{x}}_k = \mathbf{x}_{k-1} - \beta_k V S S_k^{\mathbf{D}^T} (V S S_k^{\mathbf{D}} (\mathbf{x}_{k-1}) - \mathbf{y}).$$
 (10)

Estimating the decomposed matrices (W, M) is challenging due to their mutual dependence. To handle this, we reformulate the optimization problem as:

$$\tilde{\mathbf{x}}_k = \arg\min_{\tilde{\mathbf{x}}} \frac{1}{2} \|\mathbf{y} - \mathbf{W}\tilde{\mathbf{x}}\mathbf{M}\|_2^2 + \psi_{\mathbf{W}}(\mathbf{W}) + \psi_{\mathbf{M}}(\mathbf{M}),$$
 (11)

where $\psi_{\mathbf{W}}(\cdot)$ and $\psi_{\mathbf{M}}(\cdot)$ are regularization terms for \mathbf{W} and \mathbf{M} . Since \mathbf{W} and \mathbf{M} are physically coupled, we solve them alternatively, effectively preventing gradient oscillations.

We replace $\psi_{\mathbf{W}}(\cdot)$ and $\psi_{\mathbf{M}}(\cdot)$ with learnable update functions $\mathcal{D}_{\mathbf{M}}(\cdot)$ and $\mathcal{D}_{\mathbf{W}}(\cdot)$, transforming hand-crafted priors into learnable ones. By integrating their physical interdependence within the fidelity term, the two matrices are

$$\mathbf{M}_k = \mathcal{D}_{\mathbf{M}}(\mathbf{y}, \mathbf{W}_{k-1} \mathbf{x}_k), \tag{12}$$

$$\mathbf{W}_k = \mathcal{D}_{\mathbf{W}}(\mathbf{y}, \mathbf{x}_k \mathbf{M}_k), \tag{13}$$

initialized with $\mathbf{M}_0 = N(\mathbf{y}\mathbf{y}^T)$ and $\mathbf{W}_0 = N(\mathbf{y}^T\mathbf{y})$, where $N(\cdot)$ denotes l_2 normalization for consistent scal-

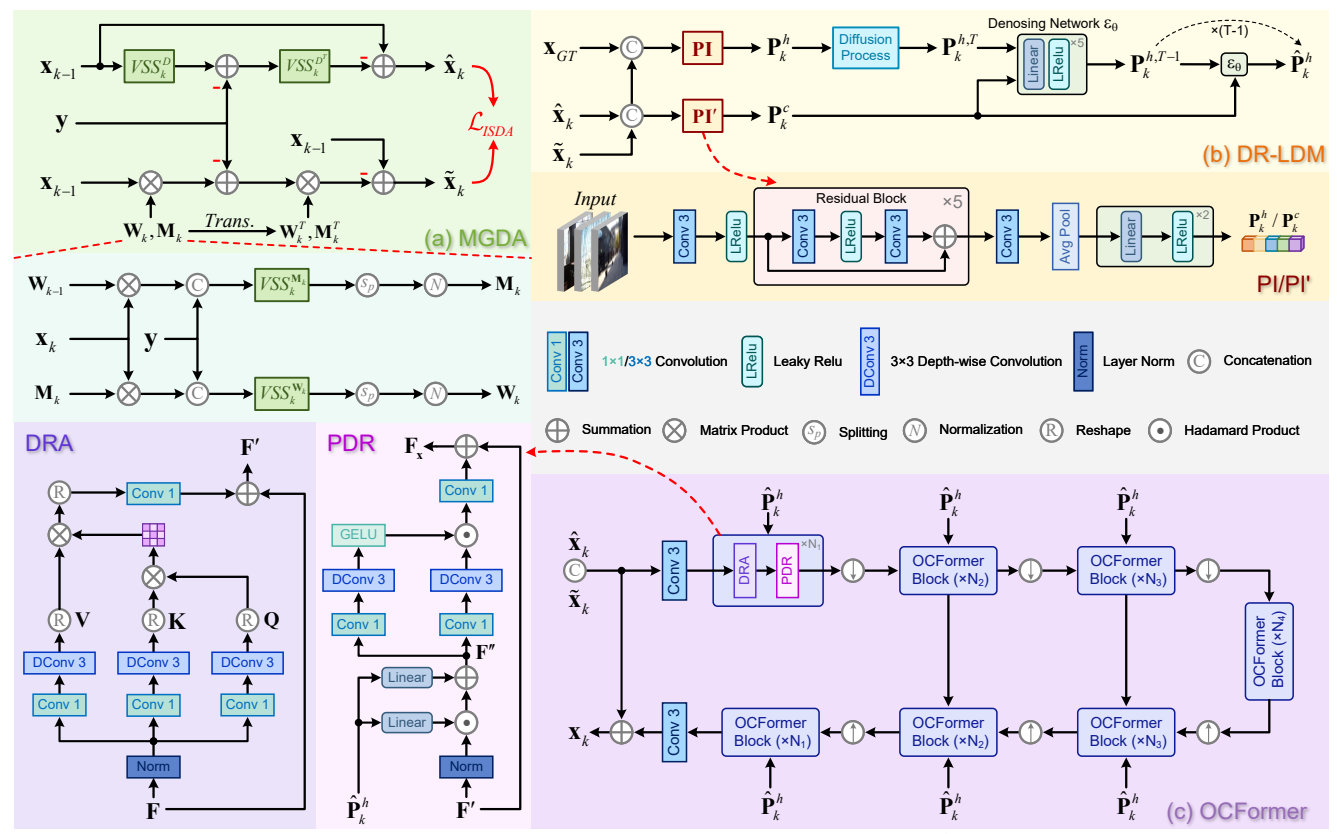


Figure 3. Details of MGDA, DR-LDM, and OCF ormer at the \boldsymbol{k}^{th} stage.

ing. To compute \mathbf{M}_k , we first estimate two half-matrix blocks, \mathbf{M}_k^1 and \mathbf{M}_k^2 , representing its left and right projections. We employ a VSS module to extract non-local correlations from the concatenation of \mathbf{y} and $\mathbf{W}_{k-1}\mathbf{x}_k$:

 $\mathbf{M}_k^1, \mathbf{M}_k^2 = S_p(VSS_k^{\mathbf{M}_k}(conca(\mathbf{y}, \mathbf{W}_{k-1}\mathbf{x}_k))),$ (14) where $S_p(\cdot)$ denotes channel-wise splitting, ensuring $\mathbf{M}_k^1, \mathbf{M}_k^2 \in \mathbb{R}^{c \times w \times w}$. We then aggregate their correlations in the embedding space, formulated as:

$$\mathbf{M}_k = N((\mathbf{M}_k^1)^T \mathbf{M}_k^2), \tag{15}$$

This encourages \mathbf{M}_k to capture statistical correlations and directional dependencies between \mathbf{y} and $\mathbf{W}_{k-1}\mathbf{x}_k$, forming a structured approximation of degradation in the latent space. \mathbf{W}_k can be calculated similarly.

Finally, the decomposed update becomes:

$$\tilde{\mathbf{x}}_k = \mathbf{x}_{k-1} - \gamma_k \mathbf{W}_k^T (\mathbf{W}_k \mathbf{x}_{k-1} \mathbf{M}_k - \mathbf{y}) \mathbf{M}_k^T, \quad (16)$$

where $\hat{\mathbf{x}}_k$ captures coarse global consistency, while $\tilde{\mathbf{x}}_k$ refines structure and local accuracy, forming a complementary optimization that balances scalability and precision.

OCFormer. Given the MGDA outputs $\hat{\mathbf{x}}_k$ and $\tilde{\mathbf{x}}_k$, we concatenate them with the clean image \mathbf{x}_{GT} and feed the combined one into the PI module (see Fig. 3 (b)), a network commonly used for learning compact latent priors [20]:

$$\mathbf{P}_k^h = \text{PI}(\text{conca}(\hat{\mathbf{x}}_k, \tilde{\mathbf{x}}_k, \mathbf{x}_{GT})), \tag{17}$$

where \mathbf{P}_k^h is a compact vector of length C_p . This concatenation allows the prior to encode the discrepancy between

clean and degraded representations, modeling degradationrelated cues. \mathbf{P}_k^h guides the OCFormer to refine $\hat{\mathbf{x}}_k$ and $\tilde{\mathbf{x}}_k$:

$$\mathbf{x}_k = \text{OCFormer}(\hat{\mathbf{x}}_k, \tilde{\mathbf{x}}_k, \mathbf{P}_k^h), \tag{18}$$

which, alike Eq. (9), serves a learnable proximal operator. OCFormer adopts a U-shaped structure with specialized blocks comprising degradation-resistant attention (DRA) and prior-guided detail recovery (PDR) modules.

We first extract feature maps \mathbf{F} from the concatenation of $\hat{\mathbf{x}}_k$ and $\tilde{\mathbf{x}}_k$ using 3×3 convolutions (the stage index k is omitted for clarity). DRA employs self-attention to capture complementary information between the two feature sets:

$$\mathbf{Q} = \mathbf{W}_Q \mathbf{F}, \ \mathbf{K} = \mathbf{W}_K \mathbf{F}, \ \mathbf{V} = \mathbf{W}_V \mathbf{F},$$
 (19)

where W combines 1×1 point-wise and 3×3 depth-wise convolutions. The self-attention output F' is given by:

$$\mathbf{F}' = S(\mathbf{Q}\mathbf{K}^T/I) \cdot \mathbf{V} + \mathbf{F},\tag{20}$$

with $S(\cdot)$ is Softmax and I a scaling parameter. To recover lost details, PDR integrates the high-quality prior \mathbf{P}_k^h :

$$\mathbf{F}_{\mathbf{x}} = \mathbf{F}' + \text{GELU}(\mathbf{W}_G \mathbf{F}'') \odot \mathbf{W}_H \mathbf{F}'', \tag{21}$$

$$\mathbf{F}'' = Linear_1(\mathbf{P}_k^h) \odot LN(\mathbf{F}') + Linear_2(\mathbf{P}_k^h), \quad (22)$$

where \mathbf{W}_G and \mathbf{W}_H share projection structures of Eq. (19). GELU(•), Linear(•), and LN(•) denote GELU activation [19], linear layers, and layer normalization, respectively. The prior reweights latent features, enhancing fine structures that existing DUNs often oversmooth.



Figure 4. Visualization of image denoising. Our method restores a sharper letter "s" in "His" (left) and a more accurate "i" in "ion" (right).



Figure 5. Visualization of image deblurring. Our method resulted in a clearer hairpin (left) and a more accurate lettering "A" (right).

Optimization. After K stages, we obtain the final result \mathbf{x}_K . Given \mathbf{x}_{GT} , the basic reconstruction loss follows [8]:

$$\mathcal{L}_{Rec} = \|\mathbf{x}_K - \mathbf{x}_{GT}\|_1. \tag{23}$$

Apart from \mathcal{L}_{rec} , MGDA estimates both holistic and decomposed degradations, which are theoretically equivalent but empirically complementary. To encourage mutual consistency without impairing this complementarity, we introduce the Intra-Stage Degradation-Aware (ISDA) loss:

$$\mathcal{L}_{ISDA} = \sum_{k=2}^{K} \frac{1}{2^{K-k}} \|\hat{\mathbf{x}}_k - \tilde{\mathbf{x}}_k\|_1,$$
 (24)

applied from the second stage onward to relax early-stage alignment. The total loss with a hyperparameter ζ_1 is:

$$\mathcal{L}_{Total}^{I} = \mathcal{L}_{Rec} + \zeta_1 \mathcal{L}_{ISDA}.$$
 (25)

4.2. Phase II: Optimize DR-LDM

In phase II, DR-LDM is trained to generate high-quality priors from MGDA outputs $(\hat{\mathbf{x}}_k, \tilde{\mathbf{x}}_k)$. The predicted prior $\hat{\mathbf{P}}_k^h$ aims to match the prior \mathbf{P}_k^h extracted by the pretrained PI. **Diffusion process**. In this process, we first use PI to extract the clean prior \mathbf{P}_k^h , which serves as the initialization of the forward Markov chain: $\mathbf{P}_k^h = \mathbf{P}_k^{h,0}$. Gaussian noise is then added across T steps. At step t, the forward process is:

$$q\left(\mathbf{P}_{k}^{h,t}|\mathbf{P}_{k}^{h,t-1}\right) = \mathcal{N}\left(\mathbf{P}_{k}^{h,t}; \sqrt{1-\beta^{t}}\mathbf{P}_{k}^{h,t-1}, \beta^{t}\mathbf{I}\right), (26)$$

where $t \in [1,T]$. $\mathbf{P}_k^{h,t}$ denotes the noisy prior at time step t and stage k. β^t is a predefined variance schedule controlling the noise strength and $\mathcal N$ is the Gaussian distribution. Following [28], we define $\alpha^t = 1 - \beta^t$ and $\bar{\alpha}^t = \prod_{i=1}^t \alpha^i$, which leads to the simplified marginal distribution:

$$q\left(\mathbf{P}_{k}^{h,t}|\mathbf{P}_{k}^{h,0}\right) = \mathcal{N}\left(\mathbf{P}_{k}^{h,t}; \sqrt{\bar{\alpha}^{t}}\mathbf{P}_{k}^{h,0}, (1-\bar{\alpha}^{t})\mathbf{I}\right). \tag{27}$$

Reverse process. In this process, DR-LDM recovers the clean prior from a Gaussian noise sample. It begins with a random initialization $\mathbf{P}_k^{h,T} \sim \mathcal{N}(0,\mathbf{I})$ and progressively denoises it to $\mathbf{P}_k^{h,0}$. Each step is modeled as:

$$p\left(\mathbf{P}_{k}^{h,t-1}|\mathbf{P}_{k}^{h,t|0}\right) = \mathcal{N}\left(\mathbf{P}_{k}^{h,t-1};\boldsymbol{\mu}^{t}(\mathbf{P}_{k}^{h,t|0}),(\boldsymbol{\sigma}^{t})^{2}\mathbf{I}\right), \quad (28)$$
where $\mathbf{P}_{k}^{h,t|0} = (\mathbf{P}_{k}^{h,t},\mathbf{P}_{k}^{h,0}), \, \boldsymbol{\mu}^{t}(\mathbf{P}_{k}^{h,t|0}) = \frac{1}{\sqrt{\kappa^{t}}}(\mathbf{P}_{k}^{h,t} - \mathbf{P}_{k}^{h,t})$

 $\frac{1-\alpha^t}{\sqrt{1-\bar{\alpha}^t}}\epsilon$), and $(\sigma^t)^2=\frac{1-\bar{\alpha}^{t-1}}{1-\bar{\alpha}^t}\beta^t$. ϵ represents Gaussian noise, which is estimated using a denoising network $\epsilon_{\theta}(\cdot)$. To stabilize the process, an auxiliary prior extraction module PI' is introduced to compute a conditional cue \mathbf{P}_k^c from the concatenation of the MGDA outputs, $\hat{\mathbf{x}}_k$ and $\tilde{\mathbf{x}}_k$, that is

$$\mathbf{P}_k^c = \mathrm{PI}'(\mathrm{conca}(\hat{\mathbf{x}}_k, \tilde{\mathbf{x}}_k)). \tag{29}$$

Hence, $\mathbf{P}_k^{h,t-1}$ is updated by setting the variance to $1-\alpha^t$: $\mathbf{P}_k^{h,t-1} = \frac{1}{\sqrt{\alpha^t}} (\mathbf{P}_k^{h,t} - \frac{1-\alpha^t}{\sqrt{1-\alpha^t}} \boldsymbol{\epsilon}_{\theta} (\mathbf{P}_k^{h,t}, \mathbf{P}_k^c, t)) + \sqrt{1-\alpha^t} \boldsymbol{\epsilon}^t$, (30) where $\boldsymbol{\epsilon}^t \sim \mathcal{N}(0,\mathbf{I})$. After T denoising steps, DR-LDM outputs the reconstructed prior $\hat{\mathbf{P}}_k^h$, which is then used to guide OCFormer for fine-detail recovery. In practice, only a few steps are required to produce a compact and high-quality prior, significantly reducing computational cost. **Optimization**. To align the predicted and ground-truth priors, we define a diffusion consistency loss:

$$\mathcal{L}_{Diff} = \|\hat{\mathbf{P}}_k^h - \mathbf{P}_k^h\|_1. \tag{31}$$

For end-to-end optimization, we jointly train all components of UnfoldLDM with the total Phase II objective:

$$\mathcal{L}_{Total}^{II} = \mathcal{L}_{Rec} + \zeta_2 \mathcal{L}_{ISDA} + \zeta_3 \mathcal{L}_{Diff}, \qquad (32)$$
 where ζ_2 and ζ_3 are two hyper-parameters.

4.3. Inference

During inference, at the k^{th} stage, UnfoldLDM takes the degradation-corrected estimates $(\hat{\mathbf{x}}_k, \tilde{\mathbf{x}}_k)$ from MGDA and employs PI' to encode the conditional prior cue \mathbf{P}_k^c . DR-LDM then synthesizes a high-quality prior $\hat{\mathbf{P}}_k^h$, which guides OCFormer to produce the restored image \mathbf{x}_k . Across successive stages, MGDA progressively refines degradation estimation, while DR-LDM and OCFormer collaboratively enhance texture recovery. This synergy ensures that the final output is both degradation-free and visually rich.

5. Experiment

Experimental setup. Our UnfoldLDM is implemented in PyTorch on an NVIDIA H200 GPU using the Adam optimizer with momentum terms of (0.9, 0.999). The initial learning rate is set to 2×10^{-4} and decayed to 1×10^{-6}

Table 1. Results on image denoising, The best two results Table 2. Results on underwater image Table 3. Results on backlit image enare in **red** and **blue** fonts, respectively. enhancement. hancement.

Methods	Sources	SII PSNR ↑	DD SSIM↑		VD SSIM↑	Methods	Sources	<i>UI</i> PSNR ↑		Methods	Sources		<i>ID</i> SSIM↑
SDAP [46]	ICCV23	37.53	0.936	38.56	0.940	U-shape [48]	TIP23	22.91	0.905	CLIP-LIT [33]	ICCV23	21.13	0.853
ADFNet [50]	AAAI23	39.63	0.958	39.87	0.955	PUGAN [5]	TIP23	23.05	0.897	Diff-Retinex [63]	ICCV23	22.07	0.861
VIRNet [65]	TPAMI24	39.64	0.958	39.83	0.954	ADP [75]	IJCV23	22.90	0.892	DiffIR [56]	ICCV23	21.10	0.835
MambaIR [18]	ECCV24	39.89	0.960	40.04	0.956	NU2Net [17]	AAAI23	22.38	0.903	AST [76]	CVPR24	22.61	0.851
TTT-MIM [43]	ECCV24	39.69	_	37.04	_	AST [76]	CVPR24	22.19	0.908	MambaIR [18]	ECCV24	23.07	0.874
DeepSN-Net [7]	TPAMI25	39.79	0.958	39.92	0.956	MambaIR [18]	ECCV24	22.60	0.916	RAVE [11]	ECCV24	21.26	0.872
DnLUT [60]	CVPR25	_	0.875	36.67	0.922	Reti-Diff [19]	ICLR25	24.12	0.910	Reti-Diff [19]	ICLR25	23.19	0.876
UnfoldLDM	Ours	40.02	0.961	40.06	0.958	UnfoldLDM	Ours	24.70	0.947	UnfoldLDM	Ours	24.97	0.910

Table 4. Results on image deblurring.

Table 5.	Results on	low-light in	nage enhancemen	ıt.
----------	------------	--------------	-----------------	-----

Methods	Sources		<i>Pro</i> SSIM↑		<i>DE</i> SSIM↑	Methods	Sources		L-v1 SSIM↑	-	² 2-real SSIM↑	LOL-v2- PSNR ↑	
UFPNet [9]	CVPR23	34.06	0.968	31.74	0.947	Diff-Retinex [63]	ICCV23	21.98	0.852	20.17	0.826	24.30	0.921
FFTformer [29]	CVPR23	34.21	0.968	31.62	0.946	CUE [69]	ICCV23	21.86	0.841	21.19	0.829	24.41	0.917
MLWNet-B [12]	CVPR24	33.83	0.968	31.06	0.932	GSAD [25]	NIPS23	23.23	0.852	20.19	0.847	24.22	0.927
MISC Filter [34]	CVPR24	34.10	0.969	31.66	0.946	AST [76]	CVPR24	21.09	0.858	21.68	0.856	22.25	0.927
FPro [77]	ECCV24	33.05	0.961	30.63	0.936	MambaIR [18]	ECCV24	22.23	0.863	21.15	0.857	25.75	0.937
DeepSN-Net [7]	TPAMI25	32.83	0.960	31.14	0.941	Reti-Diff [19]	ICLR25	25.35	0.866	22.97	0.858	27.53	0.951
MDT [3]	CVPR25	34.26	0.969	31.84	0.948	CIDNet [59]	CVPR25	23.50	0.900	24.11	0.871	25.71	0.942
UnfoldLDM	Ours	34.32	0.970	31.85	0.948	UnfoldLDM	Ours	25.58	0.912	23.58	0.886	27.92	0.957

Table 6. Results on image deraining, where we calculate parameters (M) and FLOPs (G) at the image size of 128×128 .

Methods	Sources	Para.	FLOPs	Rain	100L Rain100H		Test	100	Test	1200	Test2	2800	
Methods	Sources	raia.	TLOFS	PSNR ↑	SSIM↑	PSNR ↑	SSIM ↑	PSNR ↑	SSIM ↑	PSNR ↑	SSIM ↑	PSNR ↑	SSIM↑
DGUNet [44]	CVPR22	69.57	561.53	37.42	0.969	30.66	0.891	30.32	0.899	33.23	0.920	33.68	0.938
IR-SDE [40]	ICML23	135.30	119.10	38.30	0.980	31.65	0.904	_	_	_	_	30.42	0.891
MambaIR [18]	ECCV24	31.51	87.64	38.78	0.977	30.62	0.893	_	_	32.56	0.923	33.58	0.927
PRISM [58]	ArXiv25	_	_	36.88	0.966	30.06	0.889	30.29	0.900	32.56	0.913	33.73	0.939
DiNAT-IR [35]	ArXiv25	_	_	38.93	0.977	31.26	0.903	31.22	0.920	32.31	0.923	33.91	0.943
VMambaIR [52]	TCSVT25	25.17	137.00	39.09	0.979	31.66	0.909	_	_	33.33	0.926	34.01	0.944
DeepSN-Net [7]	TPAMI25	22.72	88.75	38.59	0.975	31.81	0.904	31.60	0.920	33.45	0.931	34.01	0.942
UnfoldLDM	Ours	26.91	87.32	39.55	0.981	32.27	0.912	32.67	0.925	34.26	0.932	34.25	0.945

following the cosine annealing [36]. The stage number K is set as 3, with all learnable parameters being shared across stages to reduce computational complexity. The vector length C_p is 64. The timestep of the diffusion model T is set as 3. The trade-off parameters in the loss function, $\zeta_1, \zeta_2, \zeta_3$, are all set to 1. For OCFormer, the number of transformer blocks at levels 1–4 is configured as [2,2,2,2].

5.1. Comparative Evaluation

We select PSNR and SSIM as evaluation metrics.

Image denoising. Following DeepSN-Net [7], we train UnfoldLDM on the training set of *SIDD* [1] and evaluate it on the testing sets of *SIDD* and *DND* [49]. As reported in Tab. 1 and Fig. 4, UnfoldLDM achieves SOTA performance, surpassing existing methods on both datasets.

Image deblurring. Following the common practice [7, 34], we train all models on the *GoPro* dataset [45] and evaluate them on the test sets of *GoPro* and *HIDE* [51]. As reported in Tab. 4 and Fig. 5, our UnfoldLDM achieves a leading place qualitatively and quantitatively, consistently outperforming existing cutting-edge approaches.

Underwater image enhancement. Following the protocol of Reti-Diff [19], we evaluate our method on *UIEB* [30].

As presented in Tab. 2, our method outperforms the second-best approach, Reti-Diff, by 3.24% on average. Together with the results shown in Fig. 6 with superior color correction, these findings demonstrate our effectiveness.

Backlit image enhancement. Following CLIP-LIT [33], we train and evaluate our model on the *BAID* dataset [41]. As shown in Tab. 3, our method outperforms the second-best approach, Reti-Diff, by 5.78% on average. Also, results shown in Fig. 6 indicates our superiority in anti-glare of the sun (left image), even surpassing the GT.

Low-light image enhancement. Following Reti-Diff [19], we evaluate our method on *LOL-v1* [54], *LOL-v2-real* [62], and *LOL-v2-syn* [62]. As shown in Tab. 5, UnfoldLDM achieves SOTA performance, outperforming the second-best method (Reti-Diff) and the third-best method (CIDNet) by 2.36% and 3.32%. Visualization presented in Fig. 6 also verify our superiority in visual fidelity.

Image deraining. Following DeepSN-Net [7], we evaluate performance on five datasets: *Rain100H* [61], *Rain100L* [61], *Test100* [67], *Test2800* [10], and *Test1200* [66]. As reported in Tab. 6, our method, with comparable efficiency, achieves SOTA results across all metrics and datasets. Results in Fig. 6 demonstrates our effectiveness in restoring

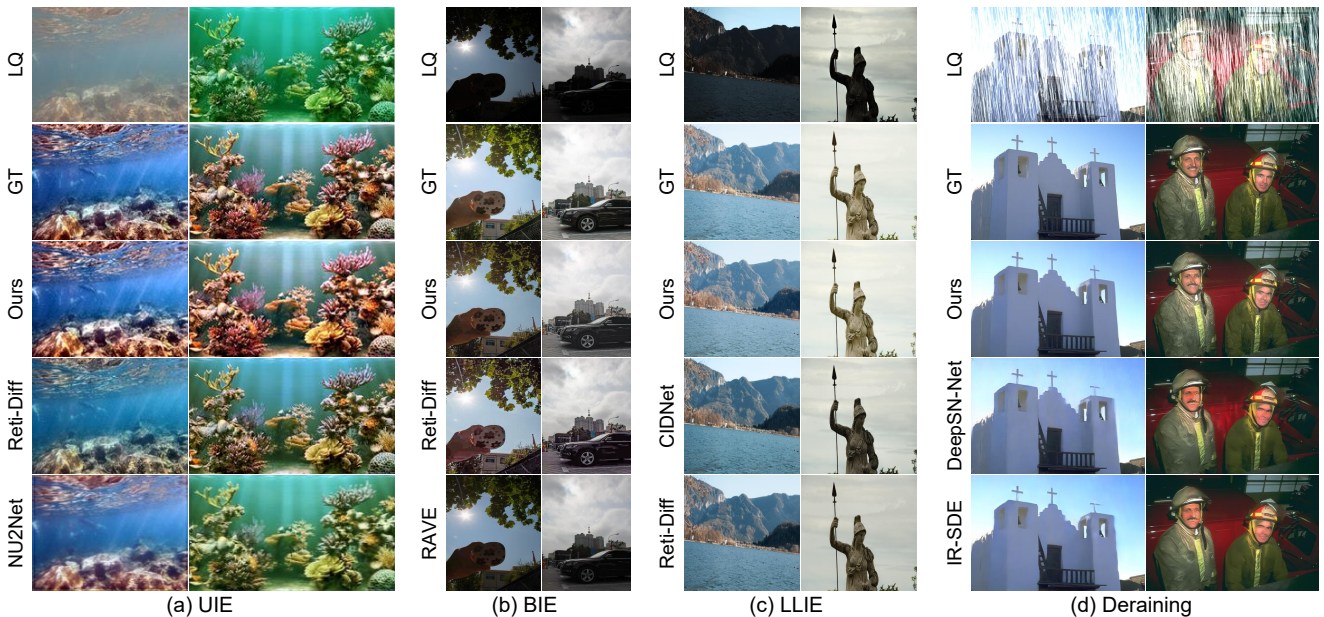


Figure 6. Visualization on UIE, BIE, LLIE, and Deraining tasks. Only SOTA methods are selected for space limitation.

Table 7. Ablation study of our UnfoldLDM.

Datacete	Metrics				N	IGDA			UnfoldLDM			
Datasets	Wictires	Retinex	w/o $\hat{\mathbf{x}}_k$	w/o $\tilde{\mathbf{x}}_k$	w/o $VSS(\cdot)$	$\mathcal{D}_1(ullet) o \mathcal{D}(ullet)$	$\mathcal{D}_2(ullet) o \mathcal{D}(ullet)$	w/o \mathcal{L}_{ISDA}	w/o DRA	w/o PDR	w/o DR-LDM	Ours
L-v2-r	PSNR	23.27	23.25	22.71	23.06	22.87	23.15	22.76	23.26	22.39	22.08	23.58
	SSIM	0.878	0.883	0.858	0.879	0.855	0.876	0.872	0.870	0.858	0.853	0.886
L-v2-s	PSNR	27.73	27.69	26.61	27.52	26.65	27.33	26.27	27.38	25.96	25.27	27.92
L-V2-3	SSIM	0.949	0.952	0.933	0.952	0.940	0.949	0.950	0.949	0.941	0.929	0.957

Table 8. Parameter analysis of the stage number K, timestep T, and vector length C_P . We also include a baseline for prior estimation using a vector of length C_P , where DR-LDM encodes only the low-quality input \mathbf{y} as the prior and uses it to guide the multi-stage network.

Datasets	Matrice		Stage nu				Times					ength C_p		Vector length C_p^1			
	Wietries	K=2	K=3	K=4	K=5	T=2	T=3	T=4	T=5	C_p =16	$C_p = 32$	C_p =64	$C_p = 128$	$C_p^1 = 16$	$C_p^1 = 32$	$C_p^1 = 64$	$C_p^1 = 128$
L-v2-r	PSNR SSIM	23.03 0.872								22.17 0.867	23.17 0.880	23.58 0.886	23.63 0.888	21.16 0.845	22.08 0.856	22.27 0.863	22.07 0.855
L-v2-s	PSNR SSIM	27.25 0.948					27.92 0.957			26.83 0.942	27.28 0.950	27.92 0.957	28.25 0.961	25.14 0.913	25.83 0.920	26.35 0.932	25.61 0.922

visual fidelity under severe raindrop occlusion.

5.2. Ablation Study

We conduct ablation study on low-light image enhancement with LOL-v2-real (L-v2-r) and $LOL\text{-}v2\text{-}synthetic}$ (L-v2-s). **Effect of MGDA**. As shown in Tab. 7, removing any of the key components, including $\hat{\mathbf{x}}_k$, $\tilde{\mathbf{x}}_k$, $VSS(\cdot)$, and \mathcal{L}_{ISDA} , causes a clear performance drop, confirming its necessity. Replacing our adaptive degradation estimation (designed for unknown degradations) with the Retinex model [55] also leads to inferior results, mainly because: (i) Retinex relies on a pretrained network with limited representational capacity, and (ii) real low-light images often involve mixed degradations beyond illumination. We further substitute our estimation functions $\mathcal{D}_{\mathbf{M}}(\cdot)$ and $\mathcal{D}_{\mathbf{W}}(\cdot)$ with alternatives: a direct network-based mapping ($\mathcal{D}_1(\cdot)$) and an SVD-based approximation ($\mathcal{D}_2(\cdot)$). The comparison highlights the advantage of modeling complex and unknown degradations.

Effect of OCFormer. As shown in Tab. 7, removing any of the core components, including DRA, PDR, or DR-LDM, leads to a performance drop, which highlights the importance of these modules.

Other configurations of UnfoldLDM. As shown in Tab. 8, our performance improves with more unfolding stages. To balance accuracy and efficiency, we set K as 3. For the timestep T of DR-LDM, we notice that T=3 already yields reliable priors, and a similar performance-efficiency trade-off is observed for the prior vector length C_p .

5.3. Further Analysis and Applications

Importance of combining DUNs with priors. We design a baseline in which DR-LDM encodes only the low-quality input as the prior to guide UnfoldLDM. As shown in Tab. 8, this configuration is highly sensitive to the prior vector length C_P^1 and tends to be unstable, as priors derived solely from degraded inputs are easily corrupted by arti-

Table 9. User study.

Table 10. Low-light image detection on ExDark.

Methods	L-v1	L-v2	UIEB	BAID	Methods (AP)	Bicycle	Boat	Bottle	Bus	Car	Cat	Chair	Cup	Dog	Motor	People	Table	Mean
Uretinex [55]	2.58	3.08	_	3.17	Baseline	74.7	64.9	70.7	84.2	79.7	47.3	58.6	67.1	64.1	66.2	73.9	45.7	66.4
CUE [69]	2.50	2.92	_		SCI [42]	73.4	68.0	69.5	86.2	74.5	63.1	59.5	61.0	67.3	63.9	73.2	47.3	67.2
MambaIR [18]	3.42	4.08	3.67	3.67	SNR-Net [57]	78.3	74.2	74.5	89.6	82.7	66.8	66.3	62.5	74.7	63.1	73.3	57.2	71.9
Reti-Diff [19]	3.58	4.17	3.50	3.58	Reti-Diff [19]	82.0	77.9	76.4	92.2	83.3	69.6	67.4	74.4	75.5	74.3	78.3	57.9	75.8
CIDNet [59]	3.17	3.92	_		CIDNet [59]	81.8	77.6	77.2	85.8	77.3	68.1	65.5	73.6	74.7	70.2	71.0	60.3	73.6
UnfoldLDM	3.92	4.25	4.08	3.83	UnfoldLDM	88.2	81.8	77.7	90.6	82.8	77.3	81.2	79.5	82.7	85.1	79.8	66.7	81.1

Table	Table 11. Generalization of UnfoldLDM, where we incorporate our DR-LDM with deep unfolding networks of different tasks.														
(a)	Low-light	image enha	ncement	(b) Image fusion						(c) Image deblurring					
Datasets M	letrics URe	tinex [55] UF	Retinex+DR-LDM	Datasets Metrics IVF-Net [26] IVF-Net+DR-LDM						tasets Metrics DeepSN-Net [7] DeepSN-Net+DR-LDM					
1-v2-r	2-r PSNR ↑ 20.44 21.93 SSIM ↑ 0.806 0.853				TNO $\begin{vmatrix} \text{EN} \uparrow \\ \text{NCC} \uparrow \end{vmatrix}$ 7.12 7.62 ${}$ 0.806 0.825		GoPro	PSNR ↑ SSIM ↑	'		33.76 0.966				
I-v2-c		24.73 0.897	26.08 0.910	INC	O EN		7.54 .811	8.13 0.829		$DE \begin{vmatrix} PSNR \uparrow \\ SSIM \uparrow \end{vmatrix} $ 31.			31.93 0.946		
	(d) I1	nage deraini	ng	(e) Salient object detection						(f) Image dehazing					
Datasets	Metrics I	OGUNet [44]	DGUNet+DR-LD	M	Datasets	Metrics	RUN [24]	RUN+DR-LDM	Datase	ets M	etrics	CORUN	N CORUN+DR-LDM		
Rain100L	PSNR ↑ SSIM ↑	38.25 0.974	38.87 0.978		DUTS	$M \downarrow F_{\beta} \uparrow$	0.022 0.886	0.021 0.898	RTTS		DE↓ SQUE↓	0.824 11.96	0.785 10.63		
Rain100H	PSNR ↑ SSIM ↑	31.06 0.897	31.89 0.905		HKU	$M \downarrow F_{\beta} \uparrow$	0.022 0.927	0.021 0.935	KIIS		SIQ-K↑ P-IQA↑	63.82 0.683	69.57 0.752		

facts. This highlights the essence of our framework: the interaction between the diffusion prior and the unfolding architecture is bidirectional. While the latent prior provides degradation-aware guidance to enhance DUN-based restoration, the DUN's coarse-to-fine optimization produces cleaner intermediate representations that, in turn, refine DR-LDM's prior learning. This mutual reinforcement allows UnfoldLDM to achieve accurate and efficient restoration across diverse degradation types.

User study. We assess the perceptual quality across lowlight (L-v1 and L-v2), underwater (UIEB), and backlit (BAID) image enhancement tasks. Twelve participants rated each enhanced image on a five-point scale (1 = worst, 5 =best) based on noise/artifacts, structural preservation, and color fidelity. Each degraded image and its enhanced version were displayed side-by-side in randomized order. As shown in Tab. 9, our method receives the highest average scores, demonstrating superior perceptual quality.

Benefits for downstream applications. We evaluate the impact of our enhanced images on low-light object detection. Following [19], enhanced results from different methods are applied to ExDark, and YOLO is retrained for each method. As reported in Tab. 10, our method achieves the best detection accuracy, confirming that the improved visual fidelity effectively benefit high-level vision understanding.

Generalization of UnfoldLDM. We further evaluate the generalization ability of UnfoldLDM by integrating the proposed DR-LDM into various deep unfolding networks across multiple restoration tasks. In this setting, DR-LDM serves as a coarse-to-fine prior generator that provides task-adaptive latent priors to guide the multi-stage optimization process. As reported in Tab. 11, consistent performance gains are observed across six representative

DUN-based models on their respective tasks, demonstrating both the versatility and superiority of our framework.

6. Conclusion

In this paper, we propose UnfoldLDM, the first to integrate DUNs with a LDM, for BIR tasks. This addresses two limitations of existing DUNs: degradation-specific dependency and over-smoothing bias. Specifically, we first introduce MGDA for robust degradation estimation. Then, we employ DR-LDM to extract the degradation-invariant prior and use the prior to guide OCFormer for explicit detail restoration. Experiments confirm the superiority of our UnfoldLDM.

References

- [1] Abdelrahman Abdelhamed, Stephen Lin, and Michael S Brown. A high-quality denoising dataset for smartphone cameras. In CVPR, pages 1692-1700, 2018. 6
- [2] Antonin Chambolle. An algorithm for total variation minimization and applications. Journal of Mathematical imaging and vision, 20(1):89-97, 2004. 2
- [3] Duosheng Chen, Shihao Zhou, Jinshan Pan, Jinglei Shi, Lishen Qu, and Jufeng Yang. A polarization-aided transformer for image deblurring via motion vector decomposition. In CVPR, pages 28061–28070, 2025. 6
- [4] Zheng Chen, Haotong Qin, Yong Guo, Xiongfei Su, Xin Yuan, Linghe Kong, and Yulun Zhang. Binarized diffusion model for image super-resolution. In NeurIPS, 2024. 1
- [5] Runmin Cong, Wenyu Yang, Wei Zhang, Chongyi Li, Chun-Le Guo, Qingming Huang, and Sam Kwong. Pugan: Physical model-guided underwater image enhancement using gan with dual-discriminators. IEEE Transactions on Image Processing, 2023. 6
- [6] Lizhen Deng, Chunming He, Guoxia Xu, Hu Zhu, and Hao Wang. Pcgan: A noise robust conditional generative ad-

- versarial network for one shot learning. <u>IEEE Transactions</u> on Intelligent Transportation Systems, 23(12):25249–25258, 2022. 1, 2
- [7] Xin Deng, Chenxiao Zhang, Lai Jiang, Jingyuan Xia, and Mai Xu. Deepsn-net: Deep semi-smooth newton driven network for blind image restoration. <u>IEEE Trans. Pattern Anal.</u> Mach. Intell., 2025. 1, 6, 8
- [8] Chengyu Fang, Chunming He, Fengyang Xiao, Yulun Zhang, Longxiang Tang, Yuelin Zhang, Kai Li, and Xiu Li. Real-world image dehazing with coherence-based label generator and cooperative unfolding network. <u>NeurIPS</u>, 2024.
- [9] Zhenxuan Fang, Fangfang Wu, Weisheng Dong, Xin Li, Jinjian Wu, and Guangming Shi. Self-supervised non-uniform kernel estimation with flow-based motion prior for blind image deblurring. In CVPR, pages 18105–18114, 2023. 6
- [10] Xueyang Fu, Jiabin Huang, Delu Zeng, Yue Huang, Xinghao Ding, and John Paisley. Removing rain from single images via a deep detail network. In <u>CVPR</u>, pages 3855–3863, 2017.
- [11] Tatiana Gaintseva, Martin Benning, and Gregory Slabaugh. Rave: Residual vector embedding for clip-guided backlit image enhancement. In <u>ECCV</u>, pages 412–428. Springer, 2024.
- [12] Xin Gao, Tianheng Qiu, Xinyu Zhang, Hanlin Bai, Kang Liu, Xuan Huang, Hu Wei, Guoying Zhang, and Huaping Liu. Efficient multi-scale network with learnable discrete wavelet transform for blind motion deblurring. In <u>CVPR</u>, pages 2733–2742, 2024. 6
- [13] Zijian Gao, Kele Xu, Huiping Zhuang, Li Liu, Xinjun Mao, Bo Ding, Dawei Feng, and Huaimin Wang. Less confidence, less forgetting: Learning with a humbler teacher in exemplar-free class-incremental learning. <u>Neural Networks</u>, 179:106513, 2024. 2
- [14] Zijian Gao, Xingxing Zhang, Kele Xu, Xinjun Mao, and Huaimin Wang. Stabilizing zero-shot prediction: A novel antidote to forgetting in continual vision-language tasks. In <u>Advances in Neural Information Processing Systems</u>, pages 128462–128488. Curran Associates, Inc., 2024. 2
- [15] Zijian Gao, Shanhao Han, Xingxing Zhang, Kele Xu, Dulan Zhou, Xinjun Mao, Yong Dou, and Huaimin Wang. Maintaining fairness in logit-based knowledge distillation for class-incremental learning. Proceedings of the AAAI Conference on Artificial Intelligence, 39(16):16763–16771, 2025. 2
- [16] Zijian Gao, Wangwang Jia, Xingxing Zhang, Dulan Zhou, Kele Xu, Feng Dawei, Yong Dou, Xinjun Mao, and Huaimin Wang. Knowledge memorization and rumination for pre-trained model-based class-incremental learning. In Proceedings of the Computer Vision and Pattern Recognition Conference, pages 20523–20533, 2025. 2
- [17] Chunle Guo, Ruiqi Wu, Xin Jin, Linghao Han, Weidong Zhang, Zhi Chai, and Chongyi Li. Underwater ranker: Learn which is better and how to be better. In <u>AAAI</u>, pages 702– 709, 2023. 6
- [18] Hang Guo, Jinmin Li, Tao Dai, Zhihao Ouyang, Xudong Ren, and Shu-Tao Xia. Mambair: A simple baseline for im-

- age restoration with state-space model. In <u>ECCV</u>, 2024. 3, 6, 8
- [19] Chunming He, Chengyu Fang, Yulun Zhang, Kai Li, Longxiang Tang, Chenyu You, Fengyang Xiao, Zhenhua Guo, and Xiu Li. Reti-diff: Illumination degradation image restoration with retinex-based latent diffusion model. <u>arXiv preprint</u> arXiv:2311.11638, 2023. 1, 4, 6, 8
- [20] Chunming He, Kai Li, Guoxia Xu, Jiangpeng Yan, Longxiang Tang, Yulun Zhang, Yaowei Wang, and Xiu Li. Hqgnet: Unpaired medical image enhancement with high-quality guidance. <u>IEEE Transactions on Neural Networks and Learning Systems</u>, 2023. 1, 2, 4
- [21] Chunming He, Kai Li, Guoxia Xu, Yulun Zhang, Runze Hu, Zhenhua Guo, and Xiu Li. Degradation-resistant unfolding network for heterogeneous image fusion. In <u>ICCV</u>, pages 12611–12621, 2023. 2
- [22] Chunming He, Kai Li, Yachao Zhang, Longxiang Tang, Yulun Zhang, Zhenhua Guo, and Xiu Li. Camouflaged object detection with feature decomposition and edge reconstruction. In CVPR, pages 22046–22055, 2023.
- [23] Chunming He, Rihan Zhang, Fengyang Xiao, Chengyu Fang, Longxiang Tang, Yulun Zhang, and Sina Farsiu. Unfoldir: Rethinking deep unfolding network in illumination degradation image restoration. arXiv:2505.06683, 2025. 2
- [24] Chunming He, Rihan Zhang, Fengyang Xiao, Chenyu Fang, Longxiang Tang, Yulun Zhang, Linghe Kong, Deng-Ping Fan, Kai Li, and Sina Farsiu. Run: Reversible unfolding network for concealed object segmentation. <u>arXiv preprint</u> arXiv:2501.18783, 2025. 2, 8
- [25] HOU Jinhui, Zhiyu Zhu, Junhui Hou, LIU Hui, Huanqiang Zeng, and Hui Yuan. Global structure-aware diffusion process for low-light image enhancement. In <u>NeurIPS</u>, 2023.
- [26] Mingye Ju, Chunming He, and Juping Liu. Ivf-net: An infrared and visible data fusion deep network for traffic object enhancement in intelligent transportation systems. <u>IEEE</u> Trans. Intell. Transp. Syst., 2022. 8
- [27] Mingye Ju, Chunming He, Can Ding, Wenqi Ren, Lin Zhang, and Kai-Kuang Ma. All-inclusive image enhancement for degraded images exhibiting low-frequency corruption. Trans. Circuits Syst. Video Technol., 2024. 1
- [28] Diederik P Kingma and Max Welling. Auto-encoding variational bayes. arXiv preprint arXiv:1312.6114, 2013. 5
- [29] Lingshun Kong, Jiangxin Dong, Jianjun Ge, Mingqiang Li, and Jinshan Pan. Efficient frequency domain-based transformers for high-quality image deblurring. In <u>CVPR</u>, pages 5886–5895, 2023. 6
- [30] Chongyi Li, Chunle Guo, Wenqi Ren, Runmin Cong, Junhui Hou, Sam Kwong, and Dacheng Tao. An underwater image enhancement benchmark dataset and beyond. <u>IEEE</u> Transactions on Image Processing, 29:4376–4389, 2019. 6
- [31] Hesong Li and Ying Fu. Fcdfusion: A fast, low color deviation method for fusing visible and infrared image pairs. Computational Visual Media, 11(1):195–211, 2025.
- [32] Hesong Li, Ziqi Wu, Ruiwen Shao, Tao Zhang, and Ying Fu. Noise calibration and spatial-frequency interactive network

- for stem image enhancement. In <u>Proceedings of the IEEE Conference on Computer Vision and Pattern Recognition Conference</u>, pages 21287–21296, 2025. 1
- [33] Zhexin Liang, Chongyi Li, Shangchen Zhou, Ruicheng Feng, and Chen Change Loy. Iterative prompt learning for unsupervised backlit image enhancement. In <u>ICCV</u>, pages 8094–8103, 2023. 6
- [34] Chengxu Liu, Xuan Wang, Xiangyu Xu, Ruhao Tian, Shuai Li, Xueming Qian, and Ming-Hsuan Yang. Motion-adaptive separable collaborative filters for blind motion deblurring. In CVPR, pages 25595–25605, 2024. 6
- [35] Hanzhou Liu, Binghan Li, Chengkai Liu, and Mi Lu. Dinatir: Exploring dilated neighborhood attention for high-quality image restoration. arXiv preprint arXiv:2507.17892, 2025. 6
- [36] I Loshchilov. Stochastic gradient descent with warm restarts. In ICLR, pages 1–16, 2016. 6
- [37] Shilin Lu, Yanzhu Liu, and Adams Wai-Kin Kong. Tf-icon: Diffusion-based training-free cross-domain image composition. In <u>Proceedings of the IEEE/CVF International Conference on Computer Vision</u>, pages 2294–2305, 2023.
- [38] Shilin Lu, Zilan Wang, Leyang Li, Yanzhu Liu, and Adams Wai-Kin Kong. Mace: Mass concept erasure in diffusion models. In Proceedings of the IEEE/CVF Conference on Computer Vision and Pattern Recognition, pages 6430– 6440, 2024.
- [39] Shilin Lu, Zihan Zhou, Jiayou Lu, Yuanzhi Zhu, and Adams Wai-Kin Kong. Robust watermarking using generative priors against image editing: From benchmarking to advances. arXiv preprint arXiv:2410.18775, 2024. 1
- [40] Ziwei Luo, Fredrik K Gustafsson, Zheng Zhao, Jens Sjölund, and Thomas B Schön. Image restoration with meanreverting stochastic differential equations. <u>arXiv preprint</u> arXiv:2301.11699, 2023. 6
- [41] Xiaoqian Lv, Shengping Zhang, Qinglin Liu, Haozhe Xie, Bineng Zhong, and Huiyu Zhou. Backlitnet: A dataset and network for backlit image enhancement. <u>Computer Vision</u> and Image Understanding, 218:103403, 2022. 6
- [42] Long Ma, Tengyu Ma, Risheng Liu, Xin Fan, and Zhongxuan Luo. Toward fast, flexible, and robust low-light image enhancement. In CVPR, pages 5637–5646, 2022. 8
- [43] Youssef Mansour, Xuyang Zhong, Serdar Caglar, and Reinhard Heckel. Ttt-mim: test-time training with masked image modeling for denoising distribution shifts. In <u>ECCV</u>, pages 341–357. Springer, 2024. 6
- [44] Chong Mou, Qian Wang, and Jian Zhang. Deep generalized unfolding networks for image restoration. In <u>CVPR</u>, pages 17399–17410, 2022. 1, 2, 3, 6, 8
- [45] Seungjun Nah, Tae Hyun Kim, and Kyoung Mu Lee. Deep multi-scale convolutional neural network for dynamic scene deblurring. In <u>CVPR</u>, pages 3883–3891, 2017. 6
- [46] Yizhong Pan, Xiao Liu, Xiangyu Liao, Yuanzhouhan Cao, and Chao Ren. Random sub-samples generation for selfsupervised real image denoising. In <u>ICCV</u>, pages 12150– 12159, 2023. 6
- [47] Jongwan Park, Kristen Hagan, Theodore B DuBose, Ramiro S Maldonado, Ryan P McNabb, Alfredo Dubra,

- Joseph A Izatt, and Sina Farsiu. Deep compressed multichannel adaptive optics scanning light ophthalmoscope. <u>Sci.</u> Adv., 11(19):eadr5912, 2025. 1
- [48] Lintao Peng, Chunli Zhu, and Liheng Bian. U-shape transformer for underwater image enhancement. <u>IEEE</u> Transactions on Image Processing, 2023. 6
- [49] Tobias Plotz and Stefan Roth. Benchmarking denoising algorithms with real photographs. In <u>CVPR</u>, pages 1586–1595, 2017.
- [50] Hao Shen, Zhong-Qiu Zhao, and Wandi Zhang. Adaptive dynamic filtering network for image denoising. In <u>AAAI</u>, pages 2227–2235, 2023. 6
- [51] Ziyi Shen, Wenguan Wang, Xiankai Lu, Jianbing Shen, Haibin Ling, Tingfa Xu, and Ling Shao. Human-aware motion deblurring. In ICCV, pages 5572–5581, 2019. 6
- [52] Yuan Shi, Bin Xia, Xiaoyu Jin, Xing Wang, Tianyu Zhao, Xin Xia, Xuefeng Xiao, and Wenming Yang. Vmambair: Visual state space model for image restoration. <u>IEEE</u> <u>Transactions on Circuits and Systems for Video Technology</u>, 2025. 6
- [53] Jian Sun, Huibin Li, Zongben Xu, et al. Deep admm-net for compressive sensing mri. NeurIPS, 29, 2016. 1
- [54] Chen Wei, Wenjing Wang, Wenhan Yang, and Jiaying Liu. Deep retinex decomposition for low-light enhancement. arXiv preprint arXiv:1808.04560, 2018. 6
- [55] Wenhui Wu, Jian Weng, Pingping Zhang, Xu Wang, Wenhan Yang, and Jianmin Jiang. Uretinex-net: Retinex-based deep unfolding network for low-light image enhancement. In CVPR, pages 5901–5910, 2022. 7, 8
- [56] Bin Xia, Yulun Zhang, Shiyin Wang, Yitong Wang, Xinglong Wu, Yapeng Tian, Wenming Yang, and Luc Van Gool. Diffir: Efficient diffusion model for image restoration. In ICCV, 2023. 1, 2, 6
- [57] Xiaogang Xu, Ruixing Wang, Chi-Wing Fu, and Jiaya Jia. Snr-aware low-light image enhancement. In <u>CVPR</u>, pages 17714–17724, 2022. 8
- [58] Pengze Xue, Shanwen Wang, Fei Zhou, Yan Cui, and Xin Sun. Prism: Progressive rain removal with integrated statespace modeling. arXiv preprint arXiv:2509.26413, 2025. 6
- [59] Qingsen Yan, Yixu Feng, Cheng Zhang, Pei Wang, Peng Wu, Wei Dong, Jinqiu Sun, and Yanning Zhang. You only need one color space: An efficient network for low-light image enhancement. CVPR, 2025. 6, 8
- [60] Sidi Yang, Binxiao Huang, Yulun Zhang, Dahai Yu, Yujiu Yang, and Ngai Wong. Dnlut: Ultra-efficient color image denoising via channel-aware lookup tables. In <u>CVPR</u>, pages 7582–7591, 2025. 6
- [61] Wenhan Yang, Robby T Tan, Jiashi Feng, Jiaying Liu, Zongming Guo, and Shuicheng Yan. Deep joint rain detection and removal from a single image. In <u>CVPR</u>, pages 1357–1366, 2017. 6
- [62] Wenhan Yang, Wenjing Wang, Haofeng Huang, Shiqi Wang, and Jiaying Liu. Sparse gradient regularized deep retinex network for robust low-light image enhancement. <u>IEEE</u> Transactions on Image Processing, 30:2072–2086, 2021. 6
- [63] Xunpeng Yi, Han Xu, Hao Zhang, Linfeng Tang, and Jiayi Ma. Diff-retinex: Rethinking low-light image enhancement

- with a generative diffusion model. In <u>ICCV</u>, pages 12302–12311, 2023. 2, 6
- [64] Xunpeng Yi, Han Xu, Hao Zhang, Linfeng Tang, and Jiayi Ma. Diff-retinex++: Retinex-driven reinforced diffusion model for low-light image enhancement. <u>IEEE Transactions</u> on Pattern Analysis and Machine Intelligence, 2025. 2
- [65] Zongsheng Yue, Hongwei Yong, Qian Zhao, Lei Zhang, Deyu Meng, and Kwan-Yee K Wong. Deep variational network toward blind image restoration. <u>IEEE Transactions</u> on Pattern Analysis and Machine Intelligence, 46(11):7011– 7026, 2024. 6
- [66] He Zhang and Vishal M Patel. Density-aware single image de-raining using a multi-stream dense network. In <u>CVPR</u>, pages 695–704, 2018. 6
- [67] He Zhang, Vishwanath Sindagi, and Vishal M Patel. Image de-raining using a conditional generative adversarial network. IEEE transactions on circuits and systems for video technology, 30(11):3943–3956, 2019. 6
- [68] Kai Zhang, Luc Van Gool, and Radu Timofte. Deep unfolding network for image super-resolution. In <u>CVPR</u>, pages 3217–3226, 2020.
- [69] Naishan Zheng, Man Zhou, Yanmeng Dong, Xiangyu Rui, Jie Huang, Chongyi Li, and Feng Zhao. Empowering lowlight image enhancer through customized learnable priors. In ICCV, pages 12559–12569, 2023. 6, 8
- [70] Yaozong Zheng, Bineng Zhong, Qihua Liang, Zhenjun Tang, Rongrong Ji, and Xianxian Li. Leveraging local and global cues for visual tracking via parallel interaction network. <u>IEEE Transactions on Circuits and Systems for Video</u> Technology, 33(4):1671–1683, 2022.
- [71] Yaozong Zheng, Bineng Zhong, Qihua Liang, Guorong Li, Rongrong Ji, and Xianxian Li. Toward unified token learning for vision-language tracking. <u>IEEE Transactions on Circuits</u> and Systems for Video Technology, 34(4):2125–2135, 2023.
- [72] Yaozong Zheng, Bineng Zhong, Qihua Liang, Zhiyi Mo, Shengping Zhang, and Xianxian Li. Odtrack: Online dense temporal token learning for visual tracking. In <u>Proceedings</u> of the AAAI conference on artificial intelligence, pages 7588–7596, 2024.
- [73] Yaozong Zheng, Bineng Zhong, Qihua Liang, Ning Li, and Shuxiang Song. Decoupled spatio-temporal consistency learning for self-supervised tracking. In <u>Proceedings of the</u> <u>AAAI Conference on Artificial Intelligence</u>, pages 10635– 10643, 2025. 1
- [74] Yaozong Zheng, Bineng Zhong, Qihua Liang, Shengping Zhang, Guorong Li, Xianxian Li, and Rongrong Ji. Towards universal modal tracking with online dense temporal token learning. <u>IEEE Transactions on Pattern Analysis and Machine Intelligence</u>, 2025. 1
- [75] Jingchun Zhou, Qian Liu, Qiuping Jiang, Wenqi Ren, Kin-Man Lam, and Weishi Zhang. Underwater camera: Improving visual perception via adaptive dark pixel prior and color correction. <u>International Journal of Computer Vision</u>, pages 1–19, 2023. 6
- [76] Shihao Zhou, Duosheng Chen, Jinshan Pan, Jinglei Shi, and Jufeng Yang. Adapt or perish: Adaptive sparse transformer with attentive feature refinement for image restoration. In

- Proceedings of the IEEE/CVF Conference on Computer Vision and Pattern Recognition (CVPR), pages 2952–2963, 2024. 6
- [77] Shihao Zhou, Jinshan Pan, Jinglei Shi, Duosheng Chen, Lishen Qu, and Jufeng Yang. Seeing the unseen: A frequency prompt guided transformer for image restoration. In ECCV, pages 246–264. Springer, 2024. 6
- [78] Tianyu Zhu, Hesong Li, and Ying Fu. Trim-sod: A multi-modal, multi-task, and multi-scale spacecraft optical dataset. Space: Science & Technology, 5:0299, 2025. 1